

Stochastic spatial energy deposition profiles for MeV protons and keV electrons

C. Udalagama,* A. A. Bettiol, and F. Watt

Department of Physics, National University of Singapore, Science Drive 3, Singapore 117542, Singapore

(Received 27 July 2009; revised manuscript received 4 October 2009; published 18 December 2009)

With the rapid advances being made in novel high-energy ion-beam techniques such as proton beam writing, single-ion-event effects, ion-beam-radiation therapy, ion-induced fluorescence imaging, proton/ion microscopy, and ion-induced electron imaging, it is becoming increasingly important to understand the spatial energy-deposition profiles of energetic ions as they penetrate matter. In this work we present the results of comprehensive yet straightforward event-by-event Monte Carlo calculations that simulate ion/electron propagation and secondary electron (δ ray) generation to yield spatial energy-deposition data. These calculations combine SRIM/TRIM features, EEDL97 data and volume-plasmon-localization models with a modified version of one of the newer δ ray generation models, namely, the Hansen-Kocbach-Stolterfoht. The development of the computer code DEEP (deposition of energy due to electrons and protons) offers a unique means of studying the energy-deposition/redistribution problem while still retaining the important stochastic nature inherent in these processes which cannot be achieved with analytical modeling. As an example of an application of DEEP we present results that compare the energy-deposition profiles of primary MeV protons and primary keV electrons in polymethylmethacrylate. Such data are important when comparing proximity effects in the direct write lithography processes of proton-beam writing and electron-beam writing. Our calculations demonstrate that protons are able to maintain highly compact spatial energy-deposition profiles compared with electrons.

DOI: [10.1103/PhysRevB.80.224107](https://doi.org/10.1103/PhysRevB.80.224107)

PACS number(s): 71.45.Gm, 34.50.Bw, 02.70.Uu, 34.80.Dp

I. INTRODUCTION

The recent upsurge in interest in focused MeV ion-beam techniques such as single-event effects,¹ proton-beam-radiation therapy,² scanning-ion-transmission microscopy,³ ion-induced fluorescence imaging, and proton-beam writing⁴ has been stimulated by recent advances in lens technology enabling the focusing of MeV ion beams to sub-100 nm dimensions.⁴ Due to the virtual absence of diffraction effects, there are no physical reasons why MeV ions cannot be focused to the nanometre level. If the stochastic ion-matter interactions allow a well-focused ion beam to retain its spatial compactness at the nanometer scale then this opens up numerous possibilities for the use of MeV ions. For instance, MeV ions can be used to induce fluorescence, enabling high spatial-resolution fluorescence imaging of thick samples such as whole biological cells. This will complement existing confocal or optical fluorescence microscopies, which are diffraction limited to around 200 nm spatial resolutions. With their significantly greater penetration depth, MeV ions could also be used for imaging thick specimens using scanning-transmission ion microscopy (STIM).³ STIM is a technique analogous to transmission electron microscopy, which is widely used for thin specimens. Thus, the central question we address here is whether or not focused MeV ion beams have the physical properties to provide alternative or even superior probes compared to electrons?

There are currently no complete studies that both address and compare the three-dimensional spatial profiles of energy deposition of energetic charged particles (electrons and ions) penetrating into matter. Many studies using analytical approximations based on energy distributions that are cylindrically symmetrical about the trajectory of the charged particle are limited because they do not consider the stochastic nature of the energy-deposition processes.⁵⁻⁹ For example, in the

work of Kobetich and Katz,⁵⁻⁷ energy-deposition profiles are calculated only for cylindrical shells around the ion trajectory. Although numerous computational simulations of charged-particle penetration have been developed, for example GEANT,^{10,11} these tend to be very complex.

The mechanisms through which a charged particle loses energy are dependent not only on the state of matter of the target material but also on the nature and speed of the impinging projectile.¹² Although there are many energy-loss channels available, including atomic excitation, atomic ionization, Auger emission, autoionization, plasmons, etc, we limit our interest here to those that dominate the energy-loss processes. The mechanisms considered here therefore are (1) elastic scattering, (2) atomic ionization, (3) atomic excitation, and (4) the generation of plasmons.

Our calculations are in the form of event-by-event Monte Carlo routines that simulate (1) charged-particle penetration and the generation of secondary electrons (δ rays), (2) the penetration of these δ rays and the subsequent production and penetration of up to four generations of electrons produced by these δ rays. Also incorporated is a model for the energy loss and energy deposition due to volume-plasmon generation. We will refer to our Monte Carlo simulation model presented in this paper as DEEP (deposition of energy due to electrons and protons).

Our results are described by spatial energy-deposition profiles (SEDP), determined from the physical interactions of electrons and protons penetrating matter. Since electron-beam writing using up to 100 keV is the most commonly available technique for nanostructuring and proton-beam writing is a new direct write lithography using MeV protons, we compare the mechanisms of the penetration of keV electrons and MeV protons into polymethylmethacrylate (PMMA),¹³ one of the most common polymer photoresist used in these processes.

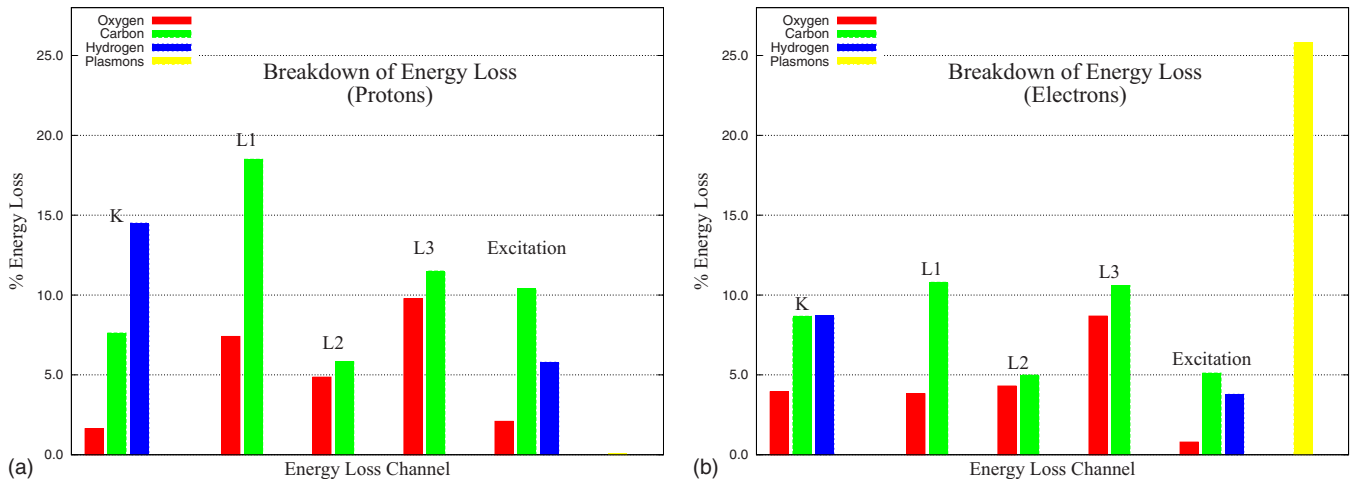


FIG. 1. (Color online) Percentage contributions to the energy loss of the primary particle from the various mechanisms. Values calculated from the simulation of Fig. 5 for 2 MeV protons and 100 keV electrons. K, L1, L2, and L3 refer to the energy lost in producing δ rays from the respective electronic shells while “excitation” refers to that energy lost in exciting the atoms.

II. CALCULATION OF SEDP'S USING DEEP

Our Monte Carlo simulation of spatial energy-deposition profiles for both electrons and ions incorporates the relevant energy loss and scattering mechanisms, namely, (1) elastic scattering from nuclei, (2) ionization, (3) excitation, and (4) plasmon generation.

A. Electrons

The cross sections necessary for the simulation of elastic scattering, ionization, and excitation for electrons are obtained from the electron-interaction-data library (EEDL97) of the Lawrence Livermore National Laboratory.¹⁴ Of the wide range of data offered in this library, the cross sections utilized in our simulations are those of large-angle elastic

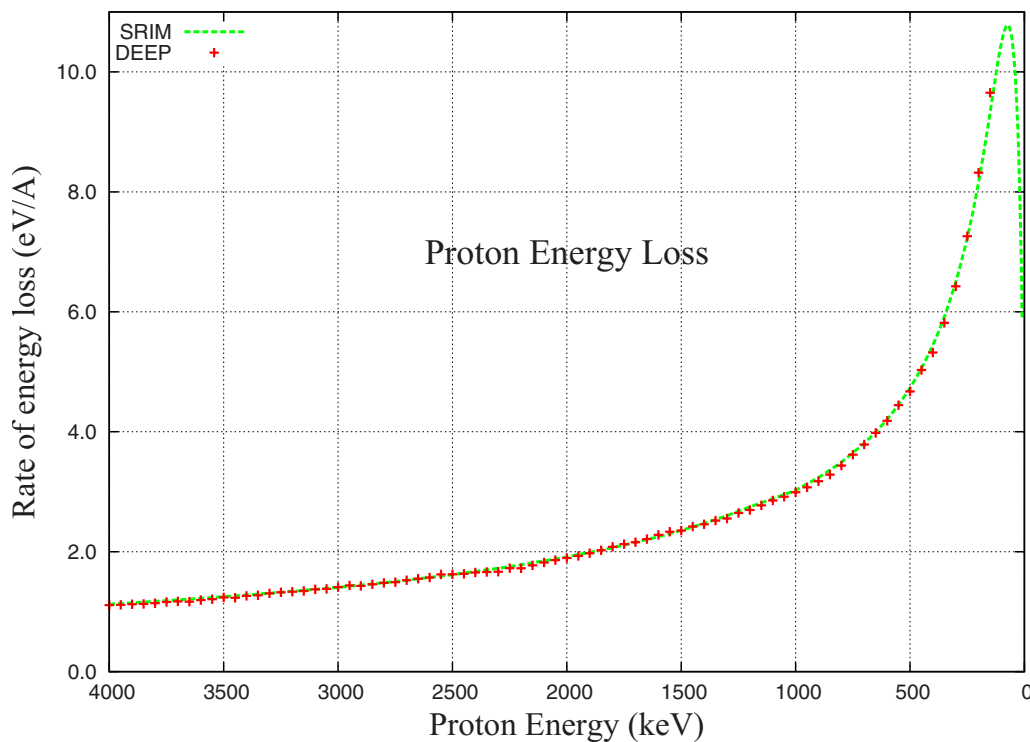


FIG. 2. (Color online) Energy loss predicted by DEEP for protons impinging into 1.19 g cm⁻³ dense PMMA. Also shown are SRIM-2008 (Ref. 27) fit of experimental data for MeV protons impinging into PMMA. DEEP employs a energy-dependant switching function to limit the energies of the lowest δ rays produced in order to arrive at an agreement between the two curves.

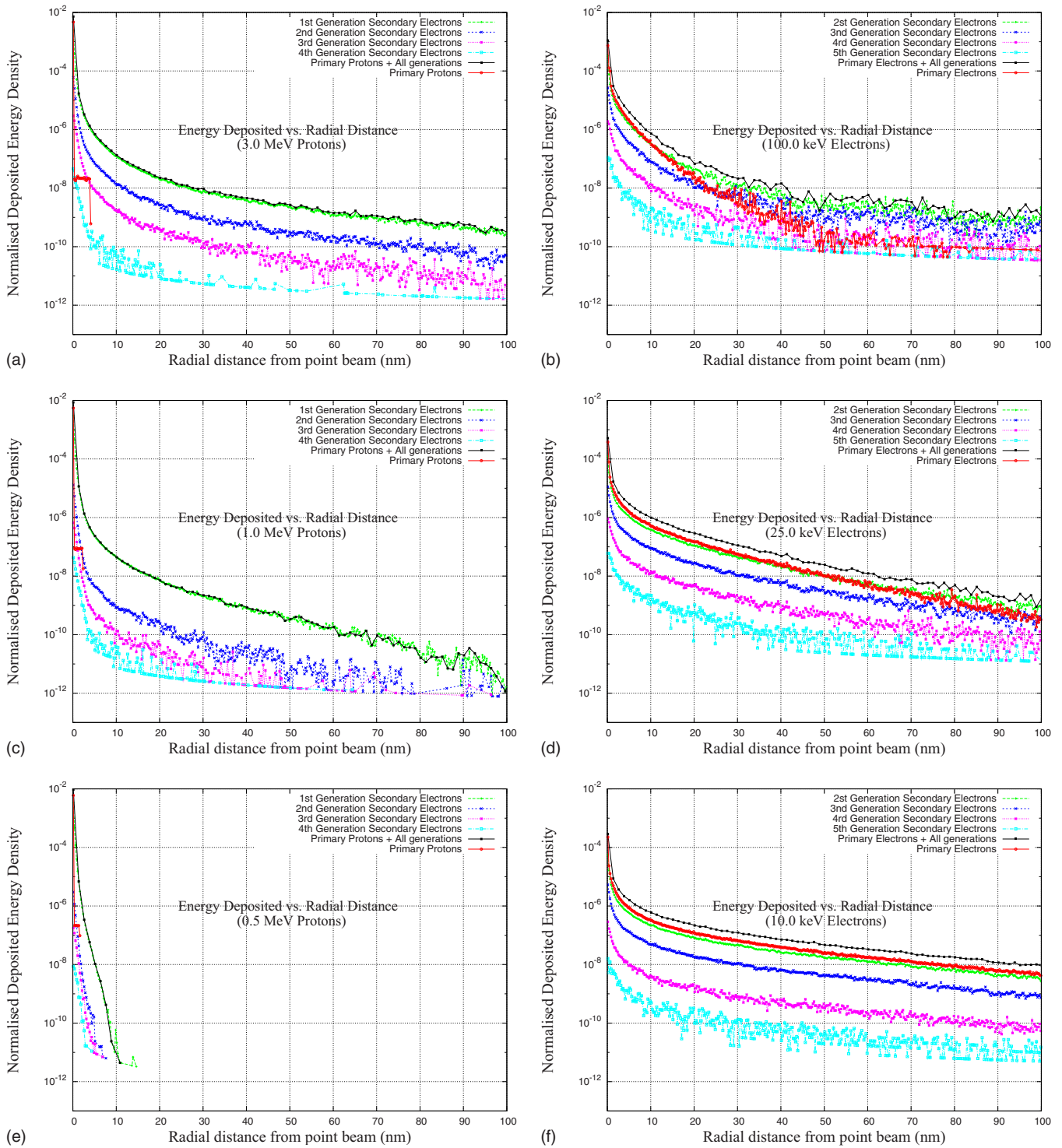


FIG. 3. (Color online) Energy deposited in a 500-nm-thick layer of PMMA using protons and electrons. The ordinates show the deposited energy density at a given radial distance away from the point beam. The figures on the left are for 0.5, 1, and 3 MeV protons and those on the right are for 10, 25, and 100 keV electrons. Shown also are the contributions from all the various generations of δ rays.

scattering, atomic excitation, and subshell ionization. The library provides cross sectional data for target Z values from 1 to 100 and incident-particle energies from 1 eV to 100 GeV, allowing DEEP to simulate relativistic electrons if required. Volume plasmons are collective longitudinal oscillations in response to a disturbance in the electron density of a material.^{15–19} Volume plasmons can be created when a

charged particle traverses the electron gas with a velocity in excess of approximately 1.3 times the Fermi velocity and are created with a specific energy-momentum relationship (dispersion in ω - k space). The generation of plasmons results in significant path deviations for electrons, which are negligible for protons. The existence of plasmons in metals has been clearly demonstrated by electron energy-loss spectroscopy.

Their existence in PMMA has also been demonstrated²⁰ although while it is clear that plasmons participate in the delocalization of energy away from the primary path of the charged particle, their role in breaking the polymeric bonds of PMMA for lithographic purposes is still disputed.^{21–23} DEEP incorporates the contributions from plasmons and the plasmon generation mean-free path used¹⁸ is

$$\frac{1}{\lambda_{plasmon}} = \left(\frac{Z_p e}{v}\right)^2 \frac{\omega_p}{4\pi\epsilon_0\hbar} \ln \frac{y}{\hbar\omega_p}, \quad (1)$$

where, ω_p is the plasma frequency given by $\sqrt{ne^2/m\epsilon_0}$ and $y=mv^2$ for electrons and $y=2mv^2$ for more massive ions. The difference in y , by a factor 2, for ions and electrons is related to the maximum exchange of momentum that can occur during a classical electron-electron (mv) and electron-ion collision ($2mv$). DEEP uses a density of 1.19 g cm⁻³ and a plasma frequency given by $\hbar\omega_p=19.81$ eV (Ref. 21) for PMMA. Note that the plasmon generation is inversely related to the particle energy so that the mean-free path for plasmon generation from MeV protons (≈ 4400 Å for 1 MeV) is much larger than for keV electrons (≈ 10 Å for 1 keV) so that plasmons are more relevant for the latter. A model for localizing these initially unlocalized excitations in water has been formulated.²⁴ As a first approximation, DEEP employs the same approach in our simulation so that the probability distribution for the localization of the plasmon energy at a distance r , from the point of generation, is given by

$$P(r)dr = e^{-(r/b_c)\gamma} \frac{r}{r^2 + b^2} dr \quad (2)$$

$b_c = \frac{v_1}{\omega_p}$, is an impact parameter describing the localization probability.¹⁷ γ is set to 5 and b to 0.2 nm as in Ref. 24.

B. Protons

There are no corresponding data libraries for protons and so our simulations are based on the following methodologies: The elastic scattering of protons from atomic nuclei is incorporated using the magic-formula impact-parameter approach adopted in the widely used SRIM/TRIM computer code.^{25–27} Although DEEP explicitly simulates these elastic events, their occurrence is rare for fast protons (e.g., 1 MeV protons in PMMA of density 1.19 g cm⁻³ have a mean-free path of ≈ 1.6 μm) and therefore these events can be neglected for energies above ≈ 90 keV.²⁸ The cross sections for proton-induced atomic excitations are obtained by scaling the corresponding electron cross sections using a $(z/v)^2$ rule, in keeping with the energy-loss description within the Born approximation.²⁸ Proton-induced δ ray production is incorporated using the cross sections from the Hansen-Kocbach-Stolterfoht (HKS) (Refs. 12 and 29–31) model, which has displayed good agreement with experimental data. We have also included the work of Bernal and Liendo³² to correct inconsistencies between the single and double differential cross-section values predicted by the HKS formalism. The formalism for proton plasmon generation is the same as that for electrons and is described above. The relevant doubly

differential cross sections used in this work are presented below. The formulae are all expressed in atomic units.

$$\frac{d^2\sigma(\theta, W)}{dWd\Omega} = \left(\frac{Z_p}{v}\right)^2 \frac{32}{3\pi\alpha_c^3} \left[\frac{1}{1 + (\tilde{K}_m - \tilde{k}_t \cos \theta)^2} \right]^3, \quad (3)$$

where

Z_p charge of the impinging particle,

B binding energy,

R Rydberg energy,

$v = \sqrt{2T}$ velocity of the impinging particle,

$T = (E/Z_p)(m_e/m_p)$ reduced kinetic energy,

$K_m = (\alpha^2 + k^2)/2v$ minimum momentum transfer,

$k = \sqrt{2W}$ momentum of outgoing δ

$\alpha = \sqrt{2B}$ mean initial momentum,

k_c, k_t, α_c small modifications to k and α ,

$$\tilde{k}_t = k_t/\alpha_c,$$

$$\tilde{K}_m = K_m/\alpha_c.$$

The expressions below for k_c, k_t, α_c are meant to optimize the model to fit in with the Born approximation.

$$k_c = \left[k^2 + \frac{2\alpha^2}{\ln\left(\frac{2v^2}{\alpha^2}\right)} \right]^{1/2},$$

$$k_t = \left(k^2 + 0.2\alpha^2 \sqrt{\frac{v}{\alpha}} \right)^{1/2},$$

and

$$\alpha_c = \alpha \left(1 + 0.7 \frac{v^2}{v^2 + k^2} \right).$$

The above doubly differential cross section can be integrated to yield the singly differential cross section

$$\sigma(W) = \left(\frac{Z_p}{v}\right)^2 \frac{8}{\alpha k_c^3 \tilde{k}_t} \left\{ \arctan(\tilde{K}_m + \tilde{k}_t) - \arctan(\tilde{K}_m - \tilde{k}_t) + \frac{5(\tilde{K}_m + \tilde{k}_t) + 3(\tilde{K}_m + \tilde{k}_t)^3}{3[1 + (\tilde{K}_m + \tilde{k}_t)^2]^2} - \frac{5(\tilde{K}_m - \tilde{k}_t) + 3(\tilde{K}_m - \tilde{k}_t)^3}{3[1 + (\tilde{K}_m - \tilde{k}_t)^2]^2} \right\}. \quad (4)$$

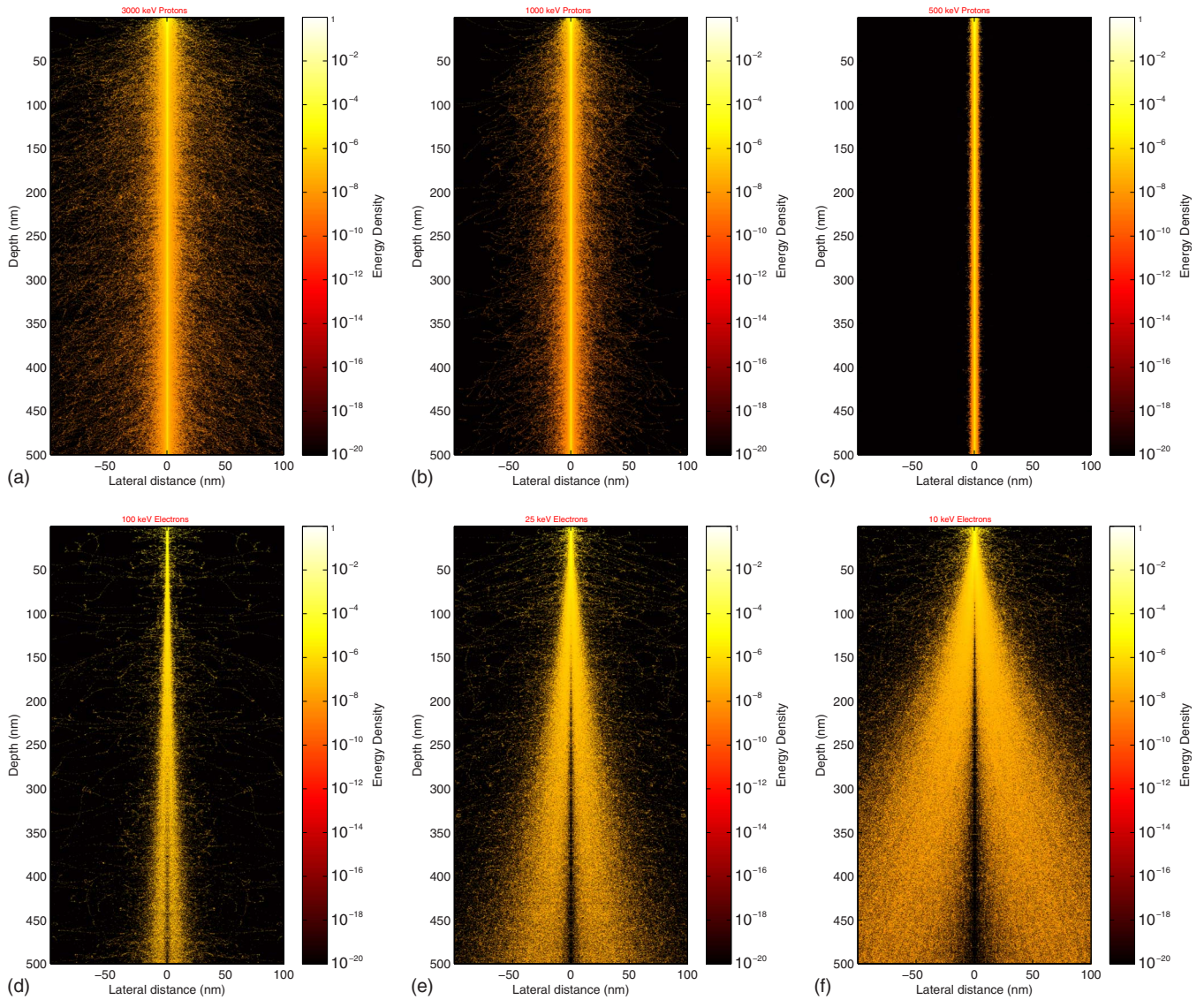


FIG. 4. (Color online) Pictorial representation of the radial deposition of energy corresponding to the data from Fig. 3. The top images correspond to 3000, 1000, and 500 keV protons while the bottom to 100, 25, and 10 keV electrons.

III. CONSTRUCTION OF THE DEEP PROGRAM

Most available Monte Carlo software tends to simulate the propagations of a particle via a continuous slowing-down approximation (CSDA), such that between any two elastic-scattering events the particle is made to lose energy continuously at a constant rate determined by experimental data or a formula; e.g., SRIM/TRIM uses a CSDA mechanism based on experimental energy-loss data. Although, this scheme is fast and simple to implement, it is difficult to incorporate the occurrence of inelastic processes and hence it is difficult to simulate how the particle loses its energy and what secondary processes it activates. We therefore have used an alternative to the CSDA approach that of simulating the particle propagation event by event^{23,31,33-35} which allows us to simulate inelastic events.

All electrons with energies greater than 10 eV and protons with energies greater than 50 keV are included. More specifically, proton propagation is simulated by modifying the

approach adopted by SRIM/TRIM, i.e., the elastic scattering (off the nuclei) is determined as in SRIM/TRIM. However, the energy loss in between two such scattering events is calculated by explicitly simulating the energy-loss events stochastically. The energy loss predicted by DEEP is adjusted so as to agree with that predicted by SRIM/TRIM. This is achieved by tuning the energy of the smallest generated δ ray. This tuning leads to the energy of the smallest δ rays being identified within 0.06–0.75 eV for PMMA. These low-energy δ rays cannot participate in any lithographic, ionization, or excitation mechanisms and being below the minimum-energy (10 eV) threshold for Monte Carlo propagation, are not included in the simulations.

DEEP can simulate energy deposition by both ions and electrons by incorporating the relevant energy-loss mechanisms of ionization, excitation, elastic scattering, and plasmon generation as described above. When an energy-deposition event occurs, that energy is allocated to a voxel,

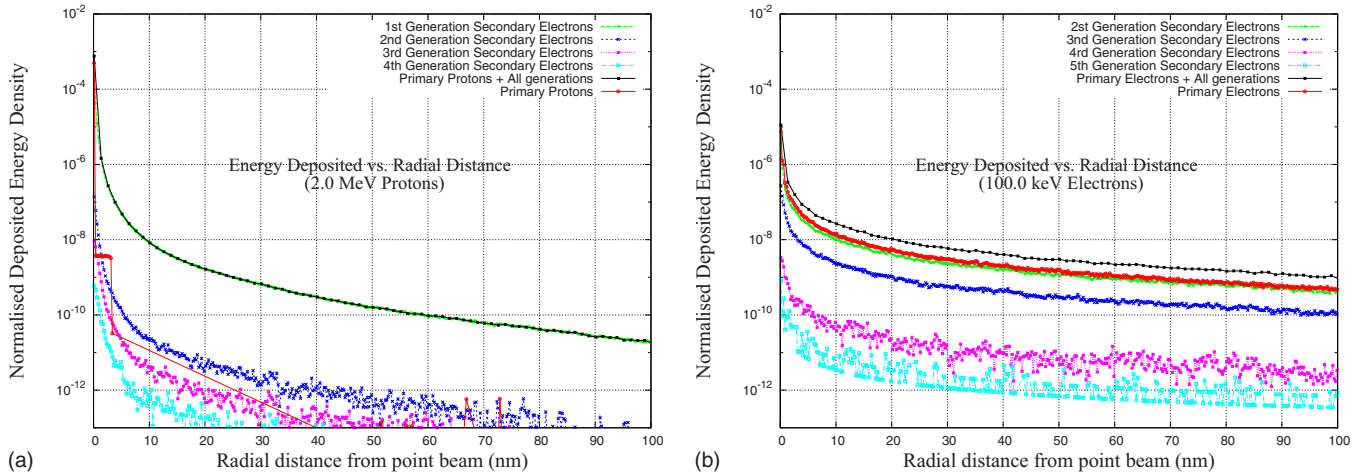


FIG. 5. (Color online) Energy deposited in a 5- μm -thick layer of PMMA using 2 MeV protons (left) and 100 keV electrons (right). The ordinates show the deposited energy density at a given radial distance away from the point beam. Shown also are the contributions from all the various generations of δ rays.

and in our simulations the voxel dimension are $0.25 \times 0.25 \times 0.25 \text{ nm}^3$.

IV. RESULTS AND DISCUSSION

The z^2/v^2 scaling of energy loss as predicted by the Born approximation implies that an electron must have approx 1850 times less energy than a proton to display an equivalent rate of energy loss. It follows therefore that the energy-deposition characteristics of 2 MeV protons used in proton-beam writing are similar to those of 1 keV electrons. Such low-electron energies however are currently of little practical interest in electron-beam lithography, where 10–100 keV electron energies are used.

Figure 1 shows the percentage contributions from various mechanisms to the energy loss of 2 MeV protons and 100 keV electrons impinging on a 5- μm -thick layer of PMMA. The main difference is the energy lost due to volume-plasmon generation, which for the electrons accounts for more than 25% of the deposited energy but is negligible for protons. This implies that the electron SEDP will tend to be broader than those of the protons as these volume plasmons transfer energy away from the initial trajectory of the primary particle.

Figure 2 shows the proton energy loss computed by DEEP for PMMA compared with the energy-loss data from SRIM-2008.²⁷ The SRIM-2008 simulation is derived from experimental energy-loss data while DEEP generates the loss stochastically from fundamental interactions. The good agreement between the SRIM-2008 results and the DEEP simulations gives us confidence in the validity of our calculations.

Figure 3 shows SEDPs simulated using DEEP for point beams of 10 000 primary protons of energies 3.0, 1.0, and 0.5 MeV and primary electrons of energy 100, 25, and 10 keV impinging on to 500-nm-thick PMMA layers. These are values typical of energies used in proton-beam and electron-beam writings. The results, which also show the contributions from each successive generation of δ rays, clearly show a smaller radial confinement of energy deposition for protons

compared with electrons. Figure 4 is a pictorial representation for the results shown in Fig. 3 and indicates the radial profile of energy deposition for the primary particles penetrating into PMMA. Interestingly, these plots show that while the proton-energy profiles are confined to a narrow radial cylinder, especially for the case of 500 keV protons, for the electron energy-deposition profiles there is an increasing radial extent with depth coupled with a shadow cone in the energy deposition centered around the primary beam axis.

Figure 5 shows the SEDPs for 2 MeV protons and 100 keV electrons penetrating deeper into a 5 μm PMMA layer. For this case, the proton SEDPs show that virtually all of the radial energy deposition is carried by the first-generation secondary electrons whereas for electrons there is a greater contribution from both the primary electrons and successive generations of δ rays. Figure 6 is a pictorial representation for the results shown in Fig. 5 and indicates that the spatial confinement for the proton radial energy deposition with depth is maintained for thick PMMA whereas the electron profiles exhibit a rapidly expanding radial profile coupled with an enhanced shadow cone.

The energy delocalization for primary protons is predominantly due to ray production and δ ray propagation. Thus, the SEDP for protons will depend on the energy spectrum of the generated δ rays. The maximum energy of the δ rays that can be ejected by 3, 1, and 0.5 MeV protons are ≈ 7 , ≈ 2 , and ≈ 1 keV, respectively, although most of the generated δ rays are made up of lower-energy electrons. As expected therefore, the most confined proton SEDP is for proton energies of 0.5 MeV, in which most of the energy deposition is contained within a few nanometres (Figs. 3 and 4) throughout the PMMA.

The energy delocalization for primary electrons however, unlike that for protons, is not limited to δ rays since the primary electrons can also be scattered with high energy. In addition, there is a greater contribution to the electron SEDP from successive generations of δ rays, which can also have significant energy. These factors, coupled with increased loss

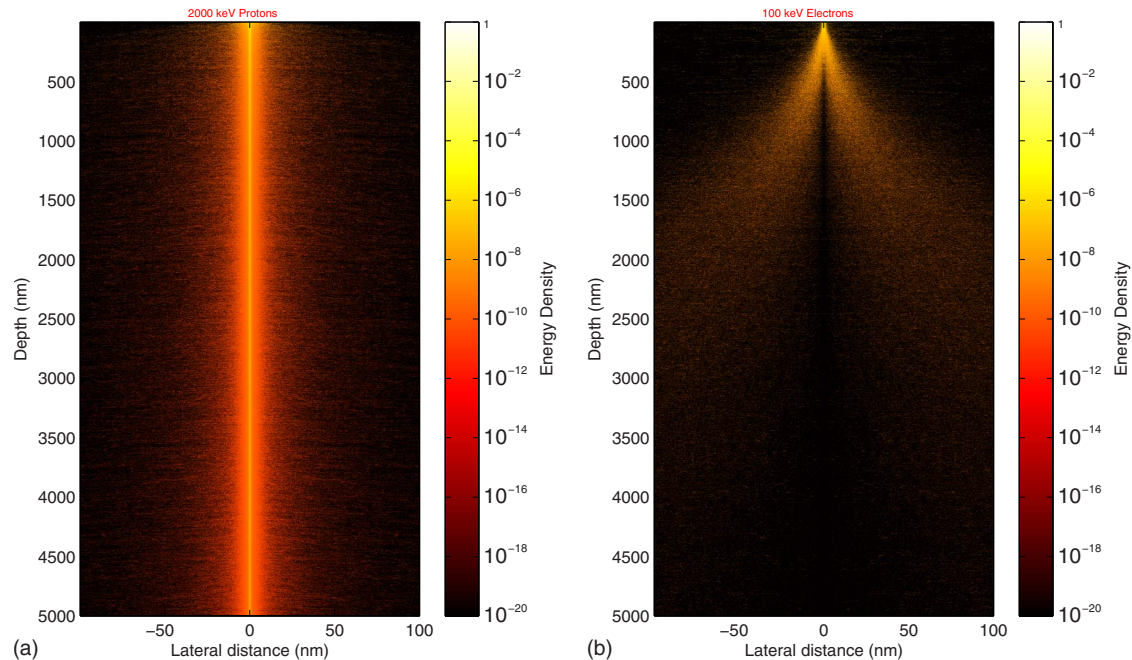


FIG. 6. (Color online) Pictorial representation of the radial deposition of energy for 2 MeV protons (left) and 100 keV electrons (right) corresponding to the data from Fig. 5 for a 5- μ m-thick layer of PMMA.

from plasmon generation, lead to a broadening of the final electron SEDP. For the case of 100 keV electrons on 5 μ m PMMA (Fig. 6) the electron SEDP is very compact at shallow depths (around several nanometres) but increases rapidly with penetration depth. In the pictorial representations in Figs. 4 and 6, there is a prominent “shadow-cone” effect observed in the electron images. This characteristic feature of the electron energy-deposition profile has been observed previously.^{36,37}

V. CONCLUSION

We have developed a comprehensive yet straightforward event-by-event Monte Carlo package that simulates ion penetration, δ ray generation, and electron penetration to yield spatial energy-deposition data. This software simulation package, DEEP, includes SRIM/TRIM features, a modified volume-plasmon-localization model, incorporates EEDL97 electron data and one of the newer ion-induced δ ray generation models, namely, the HKS. DEEP generates ion-energy loss stochastically from fundamental interactions, including the relevant secondary processes. Therefore, it is a unique yet comprehensive tool to study ion/electron energy redistribution while still retaining the inherent stochastic nature of these processes.

As an example of the application of DEEP we have pre-

sented results that compare the energy-deposition features between primary MeV protons and keV electrons in PMMA at energies relevant to proton-beam writing (≈ 0.5 –2 MeV) and electron-beam writing (≈ 10 –100 keV), which are two techniques for producing nanostructures. Our calculations have shown that protons are able to maintain spatial compactness of their SEDPs at sample depths much greater than for electrons. Electron penetration is characterized by a rapid broadening of the SEDPs with depth leading to significant, so-called, proximity effects (unintended exposure of unirradiated regions of the sample) that present problems in electron-beam lithography. In addition, the secondary electrons (δ rays) produced by penetrating protons have a much reduced spatial energy spread compared with those generated from primary electrons, thereby minimizing ion-proximity effects in comparison to electrons. Our Monte Carlo calculations therefore suggest that the potential for using protons for nanostructuring and nanoprobng down to the nanometre level is very promising.

ACKNOWLEDGMENTS

We would like to acknowledge support (Grant No. R144000227305) from the Singapore Bioimaging Consortium (SBIC—ASTAR) for funding this work.

*phycnbu@nus.edu.sg; chammika.udalagama@physics.org

- ¹J. S. Laird, T. Hirao, S. Onoda, H. Itoh, and A. Johnston, *IEEE Trans. Nucl. Sci.* **53**, 3312 (2006).
- ²S. M. MacDonald, T. F. DeLaney, and J. S. Loeffler, *Cancer Invest* **24**, 199 (2006).
- ³R. Minqin, J. A. van Kan, A. A. Bettioli, L. Daina, C. Y. Gek, B. B. Huat, H. Whitlow, T. Osipowicz, and F. Watt, *Nucl. Instrum. Methods Phys. Res. B* **260**, 124 (2007).
- ⁴F. Watt, M. B. H. Breese, A. A. Bettioli, and J. A. van Kan, *Mater. Today* **10**, 20 (2007).
- ⁵F. A. Cucinotta, R. Katz, J. W. Wilson, and R. R. Dubey, *Radial dose distributions in the δ ray theory of track structure*, AIP Conf. Proc. No. 362 (AIP, New York, 1994), p. 245.
- ⁶F. A. Cucinotta, R. Katz, J. W. Wilson, and R. R. Dubey, *NASA Tech. memo 3497*, Technical Memorandum 3497 (NASA, Houston, TX, 1995), pp. 245–265, <http://techreports.larc.nasa.gov/Itrs/itrs.html>
- ⁷E. Kobetich and R. Katz, *Phys. Rev.* **170**, 391 (1968).
- ⁸W. Stapor and P. McDonald, *J. Appl. Phys.* **64**, 4430 (1988).
- ⁹M. P. R. Waligórski, R. N. Hamm, and R. Katz, *Nucl. Tracks Radiat. Meas.* **11**, 309 (1986).
- ¹⁰S. Agostinelli, J. Allison, K. Amako, J. Apostolakis, H. Araujo, P. Arce, M. Asai, D. Axen, S. Banerjee, G. Barrand *et al.*, *Nucl. Instrum. Methods Phys. Res. A* **506**, 250 (2003).
- ¹¹J. Allison *et al.*, *IEEE Trans. Nucl. Sci.* **53**, 270 (2006).
- ¹²International Commission on Radiation Units and Measurements, *Secondary Electron Spectra From Charged Particle Interactions (ICRU REPORT 55)* (ICRU, Maryland, 1996).
- ¹³M. J. Madou, *Fundamentals of MICROFABRICATION: The Science of Miniaturization*, 2nd ed (CRC, Cleveland, 2001).
- ¹⁴S. T. Perkins and D. E. Cullen, Lawrence Livermore National Laboratory, Report No. UCRL-117796, 2002; <http://www-nds.iaea.org/epdl97>; <http://www.llnl.gov/cullen1>
- ¹⁵D. Pines, *Elementary Excitations in Solids*, Lecture Notes and Supplements in Physics (Addison-Wesley, Redwood City, CA 1963).
- ¹⁶R. A. Baragiola, C. A. Dukes, and P. Riccardi, *Nucl. Instrum. Methods Phys. Res. B* **182**, 73 (2001).
- ¹⁷R. Ritchie, R. Hamm, J. Turner, H. Wright, and J. Ashley, *Nucl. Tracks Radiat. Meas.* **16**, 141 (1989).
- ¹⁸J. Chazalviel, *Coulomb Screening by Mobile Charges*, Applications to Material Science, Chemistry, and Biology (Birkhauser, Boston, MA, 1998).
- ¹⁹E. Bonderup, *Penetration of Charged Particles Through Matter*, 2nd ed. (Institute of Physics, University of Aarhus, Aarhus, Denmark, 1981).
- ²⁰J. J. Ritsko, L. J. Brillson, R. W. Bigelow, and T. J. Fabish, *J. Chem. Phys.* **69**, 3931 (1978).
- ²¹J. P. Moliton, C. Jussiaux, T. Trigaud, R. Lazzaroni, O. Lhost, J. L. Bredas, Y. Kihn, and J. Sevely, *Philos. Mag. B* **73**, 763 (1996).
- ²²J. P. Moliton, C. Jussiaux-Devilder, T. Trigaud, R. Lazzaroni, J. L. Bredas, S. Galaup, Y. Kihn, and J. Sevely, *Philos. Mag. B* **79**, 793 (1999).
- ²³G. Han, M. Khan, Y. fang, and F. Cerrina, *J. Vac. Sci. Technol. B* **20**, 2666 (2002).
- ²⁴R. Hamm, J. Turner, R. Ritchie, and H. Wright, *Radiat. Res.* **104**, S20 (1985).
- ²⁵J. Biersack and L. Hagmark, *Nucl. Instrum. Methods* **174**, 257 (1980).
- ²⁶J. F. Ziegler, J. P. Biersack, and U. Littmark, *The Stopping and Range of Ions in Solids*, The Stopping and Ranges of Ions in Matter Vol. 1 (Pergamon, New York, 1985).
- ²⁷J. F. Ziegler and J. P. Biersack, The stopping and range of ions in matter, SRIM software, <http://www.srim.org/>
- ²⁸D. Emfietzoglou, G. Papamichaels, and M. Moscovitch, *J. Phys. D* **33**, 932 (2000).
- ²⁹J. Hansen and L. Kocbach, *J. Phys. B* **22**, L71 (1989).
- ³⁰C. N. B. Udalagama, Ph.D. thesis, National University of Singapore, 2005.
- ³¹S. Uehara, L. H. Toburen, and H. Nikjoo, *Int. J. Radiat. Biol.* **77**, 139 (2001).
- ³²M. A. Bernal and J. A. Liendo, *Nucl. Instrum. Methods Phys. Res. B* **251**, 171 (2006).
- ³³W. Wilson and H. Paretzke, *Radiat. Res.* **87**, 521 (1981).
- ³⁴W. Wilson and H. Nikjoo, *Radiat. Environ. Biophys.* **38**, 97 (1999).
- ³⁵R. Shimizu and D. Ze-Jun, *Rep. Prog. Phys.* **55**, 487 (1992).
- ³⁶M. Bolorizadeh and D. C. Joy, *J. Micro/Nanolith. MEMS MOEMS* **6**, 023004 (2007).
- ³⁷S. A. Rishton and D. P. Kern, *J. Vac. Sci. Technol. B* **5**, 135 (1987).